Multitone Waveform Synthesis With a Quantum Voltage Noise Source

Samuel P. Benz, *Fellow, IEEE*, Paul D. Dresselhaus, and Charles J. Burroughs

***Abstract*—We have developed a quantum voltage noise source (QVNS) based on pulse-driven Josephson arrays and optimized its waveform synthesis for use with Johnson noise thermometry (JNT). The QVNS synthesizes multitone waveforms with equal amplitude harmonic tones and random relative phases in order to characterize the amplitude–frequency response of the analog and digital electronics of the JNT system. We describe the QVNS circuit design and operation, including the lumped-array Josephson-junction circuit and the unipolar bias technique. In particular, we describe the primary design considerations that determine the voltage accuracy of the harmonic tones.**

***Index Terms*—Correlation, digital–analog conversion, Josephson arrays, Johnson noise, noise measurement, quantization, thermometry.**

I. Introduction

THE FIRST ac and dc voltages synthesized by a Josephson arbitrary waveform synthesizer (JAWS) were produced with unipolar pulses of a single polarity and small output voltages of less than 10 mV [1], [2]. Since then, there have been many improvements in bias technique and circuit design that increased the output rms voltage to 250 mV, which enabled quantum-accurate characterization of the ac–dc voltage response of thermal converters [3]. In order to emphasize different applications, the quantum-based pulse-driven Josephson synthesizer has used different names, including the pulse-driven Josephson digital-to-analog converter (JDAC), the ac Josephson voltage standard (ACJVS), and JAWS [1], [2]. The primary focus and development challenge for JAWS has been to produce dc and sine-wave waveforms with the largest possible voltages, which require a large number of Josephson junctions.

This paper describes a low-voltage realization of JAWS called the quantum voltage noise source (QVNS), which was developed specifically for the application of Johnson noise thermometry [4]–[6]. In contrast to the typical JAWS system, the QVNS produces multi-tone pseudo-noise waveforms with small ($< 1\ \mu$V peak) voltage amplitudes that require only a few Josephson junctions.

Johnson noise thermometry (JNT) is a primary thermometry technique based on the Johnson–Nyquist noise of a resistor, which is a fundamental result of the fluctuation–dissipation theorem. The Nyquist equation states that the mean-square voltage is proportional to Boltzmann's constant k, temperature T, resistance R, and measurement bandwidth Δf : $\langle V^2 \rangle = 4kTR\Delta f$ [7], and it is accurate to 1 part in 10^6 for frequencies below 1 MHz and temperatures above 25 K. Because the relation is fundamental, JNT is one of the few techniques that can determine absolute (thermodynamic) temperatures. NIST developed the QVNS-JNT system to investigate deviations of the International Temperature Scale of 1990 (ITS-90) from thermodynamic temperature at temperatures in the range of 505 K–933 K, which overlaps the ranges of both acoustic gas-based and radiation-based thermometry [8]. Another application of the QVNS-JNT system is as an "Electronic Kelvin" that links the SI kelvin to quantum-based electrical measurements [9]. Research is underway [10]–[16] to produce an electronic determination of Boltzmann's constant with a combined uncertainty of 6 μK/K.

The main challenge of JNT is that it requires accurate, low-noise, cross-correlation techniques to measure the extremely small $\sim 1.2\ \mathrm{nV/Hz^{1/2}}$ noise voltage of a 100 Ω resistor at the triple point of water (273.16 K) [7]. Cross correlation is necessary for these measurements because the small noise voltage is comparable to that of low-noise amplifiers. The small voltage also determines the design voltage of the QVNS synthesized waveforms. Our QVNS-JNT system uses the switched digital cross-correlator [4], [7], which was first implemented by Brixy *et al.* [17]. In cross-correlation, a signal is simultaneously measured with two separate amplifier chains. Continued integration of the cross-correlated signals gradually reduces the uncorrelated white noise of the independent amplifier chains to reveal the source signal [7], [11], [17]. The switched correlator includes a switching network at the input leads of the electronics to alternately measure the source or the reference. In a digital correlator, analog-to-digital converters (ADCs) digitize the signals from each channel and allow Fourier analysis of all signals.

For typical JNT, the reference is usually a resistor at the triple point of water, and the sense resistor is at the unknown temperature to be measured. For the NIST system, the QVNS provides an intrinsically accurate voltage reference, which characterizes the amplitude–frequency response of the cross-correlation electronics. The sense resistor can be measured at various temperatures for temperature scale characterization, or it can be measured at the triple point of water to measure Boltzmann's constant. The QVNS-JNT system is particularly useful for measuring arbitrary temperatures, not just those at fixed points; because the QVNS waveform voltage is intrinsically accurate and fully programmable with respect to spectral content and amplitude, it makes an accurate reference that allows the JNT system to measure a wide range of temperatures.

A QVNS pseudo-noise waveform is a "comb" of harmonic tones that are equally spaced in frequency (typically odd consecutive tones) and have identical amplitudes and random rel-

Manuscript received August 03, 2010; accepted September 27, 2010. Date of publication November 09, 2010; date of current version May 27, 2011. This work was supported by the National Institute of Standards and Technology. It is a contribution of the U.S. government that is not subject to U.S. copyright.

The authors are with the National Institute of Standards and Technology, Boulder, CO 80305 USA.

Digital Object Identifier 10.1109/TASC.2010.2083616

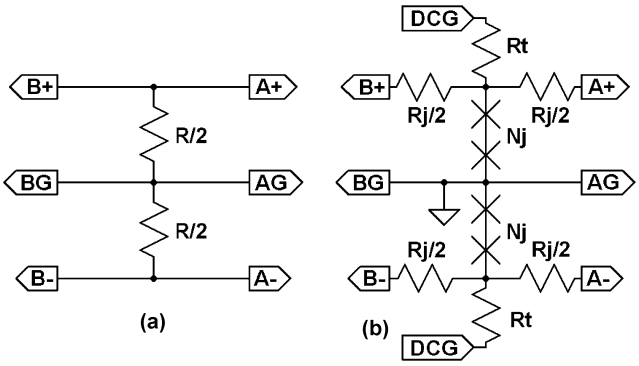

Fig. 1. (a) Resistor and (b) QVNS output wiring circuits for two-channel JNT cross-correlation measurements.

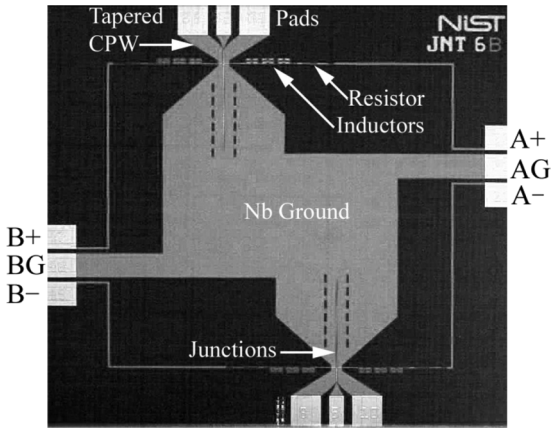

Fig. 2. Microscope photo of the QVNS chip $(1\ \mathrm{cm})^2$ with lumped Josephson arrays and low-inductance common ground (center). DCG biases are applied at the coplanar waveguide (CPW) launches (top and bottom). The three-terminal output leads for each channel are on each side.

ative phases [4], [10]. The accuracy of the QVNS waveform is provided by digital synthesis that is based on the perfectly quantized voltage pulses of Josephson junctions [1], [2]. The time-integrated area of every Josephson pulse is precisely equal to the flux quantum, $h/2e$, the ratio of Planck's constant to twice the electron charge. Knowledge of the number of pulses and their position in time is sufficient to precisely determine the voltage of any synthesized waveform. The remainder of this paper will describe the features and characteristics of the QVNS and its synthesized waveforms, including some of the issues and considerations relevant to their optimization for JNT.

II. Circuit Design

The QVNS circuit design is primarily determined by the three-wire input configuration of the low-noise preamplifiers [7], [12], which are inherently differential. Fig. 1 shows the electrical schematic of both the sense resistor and the QVNS circuits. Three wires are used in each channel (A and B) for the differential pair and ground. Both the sense resistor (typically $R = 100\,\Omega$) and the QVNS junctions (typically $2Nj = 8$, 20 or 512 junctions) are equally divided with respect to ground. Complementary pulse bias signals provided by the digital code generator (DCG) drive each array of N_j junctions to produce the opposite polarity waveforms.

The common microwave ground for each array (triangle) is also the common ground for the QVNS output leads. This common ground is essential for removing common mode signals in the QVNS circuit, either from termination resistors or from inductance in any connecting leads between the two arrays. This common ground significantly reduces the common mode signals as compared to the JAWS circuit that was used in our earliest measurements, which used two long distributed arrays and a long superconducting wire that connected them as ground [6].

The two arrays can be directly grounded to the common ground (instead of the termination resistor) because they are "lumped", which means that their physical length is much smaller than the wavelength of the 5 GHz clock period of the pulse bias waveforms [2], [18]. Since the arrays are lumped, their junctions respond identically to the pulse bias. The 50 Ω termination resistance (R_t) for the microwave transmission line of each array can reside on the DCG side of each directly grounded lumped array (as shown in Fig. 1). We have made QVNS circuits both with and without the termination resistor. Both circuits produce waveforms with satisfactory "operating margins", which are the current ranges over which various arrays maintain quantum accuracy. For recent measurements, we typically use the circuits without the termination resistor, because larger pulse current amplitudes can be provided by the DCG. Room-temperature 6 dB attenuators are used in the DCG coaxial connections to damp reflections.

Fig. 2 shows a micrograph of the QVNS circuit layout. The DCG signals are applied at the top and bottom of the chip to each set of three bright-colored Au–Pd pads, which define the beginning of the coplanar waveguide (CPW) structures, which extend vertically from both center pads. All the wiring on the chip is Nb (gray color). The Nb extending from the chip center is the low-inductance superconducting common ground. The ground extends to the center pad of each channel's output leads (at the left and right chip edges) and to the outer two pads of the CPW.

The CPW conductors are tapered to preserve the 50 Ω impedance such that the center conductor width reduces to 16 μm. The termination resistor, if present, forms the center conductor between the tapered CPW and the output lead connection. The Nb center conductor remains continuous for circuits not using the termination. Six slots in the Nb ground are on either side of the array CPW to reduce magnetic fields in the junctions. Rectangular $\mathrm{Nb{-}Nb_{.2}Si_{.8}{-}Nb}$ junctions, which are $7\ \mu\mathrm{m} \times 14\ \mu\mathrm{m}$ in area, are distributed at 10 μm intervals along the CPW center conductor. A 256 junction array fits between the output lead connection and the ground at the bottom edge of the farthest slots. Shorter arrays with four or 10 junctions (for the 8 and 20 junction QVNS chips) have a shorter CPW where the common ground is closer to the CPW pads.

The output leads for each channel (left and right chip edges) connect perpendicularly from each side of the CPW to the vertical CPW center conductor and cross under the CPW grounds in a Nb base electrode layer. To improve operating margins, each output lead contains three pairs of damped counter-wound inductive coils (closest to the CPW) to provide a high-impedance for the high speed DCG signals [19]. The 600 μm-long $(Rj/2)$

resistors reside next to these filters followed by a long superconducting lead to the output pads.

The junction critical currents are typically around $I_c = 6\,\mathrm{mA}$. Their characteristic frequencies $(2eI_cR_n/h)$ are designed to be on the order of the 5 GHz pulse frequency. Junction resistances R_n are typically around $1\ \mathrm{m\Omega}$. The above junction parameters and microwave design maximize the current range, or "operating margins", of the arrays for the pulse-drive DCG bias. The QVNS is a very reliable part of this experiment and can run continuously until the liquid He level in the dewar drops below the level of the chip (for about three weeks for a 100 l dewar).

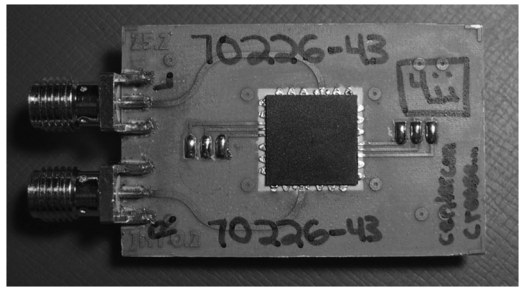

Fig. 3. Flip-chip packaging for the QVNS chip, whose pads are soldered directly to pads on the flexible carrier (back side of the chip faces out).

III. Frequency Response

A. Output Leads

In order to match the frequency response of the resistor and QVNS, their output leads should have the same capacitance (and inductance) and their circuits should have the same resistance [10], [12]. Shorter output leads with lower capacitance will increase the bandwidth of the measurement. In the sense resistor circuit, a single resistor $(R/2)$ terminates two output leads, one for each channel (A+ and B+). In the QVNS circuit, each output lead has a separate, independent resistor $(R_j/2)$. Acting as a perfect voltage source, the Josephson junctions behave as a short circuit that decouples the two (A and B) output circuits. Therefore, the QVNS output lead resistance should be twice that of the resistor circuit, $R_j = 2R$, or 100 Ω for each lead. Fortunately, the large QVNS output resistances do not significantly increase the uncorrelated noise in the QVNS measurement, because the resistors are at 4 K, not room temperature. All the output lead parameters affect the frequency response as well as the JNT measurement uncertainty [10]. In practice, trimming resistors and appropriate choice of cable lengths allow the QVNS output parameters to be matched to those of the sense resistor circuit over the 1 MHz Nyquist bandwidth of the measurement [12]. This allows the QVNS to be matched to the sense resistor for both the noise voltage, through waveform synthesis, and frequency response.

B. Nonlinearities and Packaging

Much of the recent JNT research has focused on measuring and reducing nonlinearities in the JNT electronics [12]–[16], some of which is intrinsic to the amplifiers and ADCs. It is important to reduce the nonlinearities, because the associated distortion limits the measurement uncertainty. Single-tone, dual-tone and multi-tone waveforms, and in particular odd-only and even-only tone waveforms, synthesized with both the QVNS and JAWS (for higher voltages) are excellent tools for determining the dominant sources of distortion because of their inherently low distortion. However, in our earliest QVNS and JAWS measurements, some of the largest sources of distortion in the QVNS circuits were the connections between the chip pads and the output wiring.

The first connections we used were pressed contacts between the chip pads and Au-plated BeCu spring fingers. Dirt and condensation (leading to ice) degraded the integrity of the Au–PdAu connections, and produced distortion from the resulting nonlinearities. Wire bond connections were also attempted, but were also found to produce distortion. We did not attempt to optimize the wire bonds or determine whether the nonlinearities were caused by kinks in the wires or poor connections. Instead, we developed a cryogenically robust and reliable interface based on directly soldered connections. This "flip-chip on-flex" packaging is now used as standard NIST packaging for all Josephson voltage standard chips [20].

Fig. 3 shows a typical package that is used for QVNS circuits. The flexible microwave-compatible material, which has metal on both sides, is patterned to define the microwave and output lead circuits. The DCG signals are applied through semi-rigid coax to the two SMA connectors, which connect to microstrip lines on the flex. The ground (not shown) from the back side of the carrier connects through vias to wiring pads near the chip. The three output pads on either side of the chip are connected by copper tracks on the flex to large solder bumps, which attach to low-capacitance Teflon-insulated output leads (not shown).

IV. Unipolar Waveform Synthesis

Digital codes for the QVNS pseudo-noise waveforms are generated through analog-to-digital software conversion with delta–sigma modulation algorithms [21]. The tone spacing and lowest harmonic frequency of the multi-tone waveforms are determined by the pattern repetition frequency, $f_1 = f_\mathrm{s}/M$, where f_s (typically 10 GHz) is the non-return-to-zero (NRZ) sampling frequency and M is the length of the digital code. For unipolar waveforms with NRZ clocking, all even bits of every code are defined as a "0" in order to produce RZ pulses for every "1" bit. The DCG code lengths and sampling frequency are chosen so that harmonic tones are commensurate with the frequency bins of the 2^{21} point FFTs of the waveforms, which are sampled at a 2.083 MSa/sec. A typical 25 million bit $(M = 3 \times 2^{23})$ code length corresponds to $f_1 = 397.36$ Hz, which corresponds to bin 400 of the FFT.

The typical pseudo-noise waveform is a series of odd equal-amplitude harmonic tones, $f_1, 3f_1, 5f_1, \ldots$, which have random relative phases. We typically synthesize waveforms that contain harmonic tones up to 4 MHz, which is twice the ADC sampling frequency. The rms voltage amplitude V of each tone (typically 34.6 nV) is chosen so that the synthesized waveform's average voltage noise density $V_Q = \langle V \rangle / B^{1/2}$ matches that of the thermal noise voltage, $(4kRT)^{1/2}$, to within 0.05%, where B is the tone spacing (typically $B = 2f_1$ for odd- or even-tone waveforms). The maximum quantized-step voltage of a pulse-driven series array of junctions is $V_p = nN_Jf/K_{J-90}$, where n is

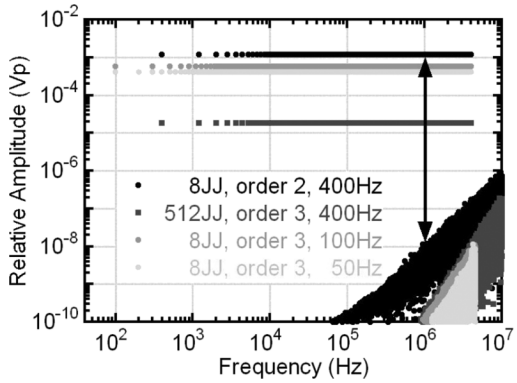

Fig. 4. The first 10 MHz of representative QVNS spectra calculated from digital code sequences. The legend indicates for each code the number of junctions (N_J), the modulator order, and the pattern repetition frequency (f_1).

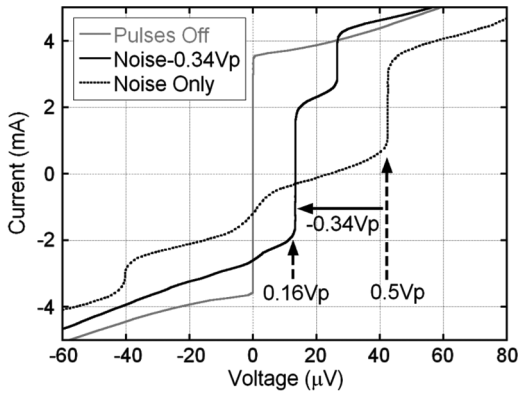

Fig. 5. Current–voltage characteristics of an 8 junction QVNS circuit without (gray) and with two different bias waveforms applied. The code that produced the middle curve (solid black line) contains an intentional negative dc voltage to reduce the inherent dc voltage of the unipolar pulses and allows the operating margins to be centered at zero current after appropriate adjustment of the pulse amplitude.

the number of quantized output pulses per input pulse (typically 1), $f = f_s/2$ is the RZ clock frequency of the pulses, and K_{J-90} is the Josephson constant (the 1990 SI defined value of $2e/h$). The calculable voltage noise of the QVNS waveform, $V_Q = QN_J(Mf_s)^{1/2}/K_{J-90}$, is represented by defined fundamental constants and integers, except for the clock frequency and Q (typically 1.480×10^{-4}). Q is the dimensionless fraction of V_p used in the delta–sigma modulator algorithm to scale the amplitude so that it produces the desired voltage noise ($V_Q \approx 1.228000\ \mathrm{nV/Hz^{1/2}}$ matches the voltage noise of a 100 Ω resistor at the triple point of water).

Fig. 4 shows FFTs of four digital codes that were designed for different waveforms, numbers of junctions, harmonic tone density (or spacing), and modulator order. The first three spectra are from odd-tone patterns, while the last $(f_1 = 50\ \mathrm{Hz})$ is from an even-tone pattern. The upper branches (horizontal points) of each FFT show the peak normalized amplitudes of the desired synthesized harmonics up to 4 MHz. The lower branches show the remaining harmonics, which represent the "digitization" or "quantization" harmonics that are a result of the modulator algorithm's analog-to-digital conversion. Note that the quantization error for every pattern is 2×10^5-times lower than the amplitude tones in that pattern for all frequencies below 1 MHz.

A. Pulse Bias Techniques

The unipolar pulse-bias technique that is typically used for QVNS synthesis is very similar to that used in the first demonstrations of pulse-driven Josephson waveform synthesis [1]. As a result of the RZ nature of the pulses, the two (0 and 1) levels of the modulator algorithm correspond to the junction voltages 0 V and V_p. The maximum peak-to-peak voltage amplitude of a unipolar waveform (V_p) can be produced only when it also contains a dc signal of amplitude $0.5V_p$. In practice, the modulator algorithm synthesizes the digital code between bipolar ± 1 levels and the zero padding even bits that are added later to the code (doubling the code length) to produce the unipolar behavior and the resulting dc voltage.

Fig. 5 shows current–voltage characteristics of a typical QVNS array with and without applied codes. For this circuit, the junction critical currents are $I_c \approx 5.8\ \mathrm{mA}$, and the average junction resistance is $R_n = 0.63\ \mathrm{m\Omega}$. When all the Josephson junctions generate exactly one quantized voltage pulse $(n = 1)$ for every pulse of the code, the array accurately produces the correct ac and dc voltage of the synthesized waveform. This current range is the operating margin of the device. The "noise only" curve in Fig. 5 shows a constant dc voltage at 41.36 μV $(0.5V_p)$ that is maintained over about 2 mA. As is typical with unipolar pulse biases, the current range and position of the quantized step is a function of pulse amplitude [1], [2]. They are also a function of pulse density.

Operating margins also generally increase for smaller pulse density. The pulse density of the QVNS codes are typically decreased by adding a negative dc offset to the code $(-0.34V_p)$, which produces larger margins. This effect is demonstrated in the middle curve, which has 3.5 mA margins and a lower 13.23 μV dc voltage. The dc offset "trick" is possible because the peak amplitude of the time-dependent noise waveforms is on the order of 10 μV ($\approx 201 \times V$ for the 5033 tones of this waveform's particular phase realization). The lower dc voltages, by use of the offset and fewer junctions in the arrays, allowed us to eliminate the dc blocking capacitors at the inputs of the preamplifiers. Large dc voltages at the preamplifier input are undesirable, because the preamplifier response can be different and may not match that of the resistor signal.

The synthesized noise waveforms produced with these two different codes are identical, except for their dc voltages. They are also produced with the same pulse bias amplitude. The pulse amplitudes are adjusted for each array so that the margins of the low-voltage waveform are centered on the zero current axis. This "self-biasing" technique (adding an intentional dc offset to the waveform and adjusting pulse amplitude) eliminates the need for additional dc biasing of the QVNS circuit to place it on operating margins.

The lower pulse amplitude is also important for reducing a potential systematic error in the QVNS output signal. The transmission line inductance of the Josephson array can produce a voltage error signal, because the pulse bias waveform has current signals at the harmonic tones. Larger pulse amplitudes would produce larger inductive voltages. Fortunately, this error

is proportional to frequency, and becomes significant only at frequencies above 100 kHz [1]–[3]. Multiple dc blocks with cut-off frequencies above 250 MHz are used on the DCG inputs to attenuate these error signals, so they are not measurable up to 1 MHz in the QVNS circuits. Removing these bias signals only slightly reduces the operating margins, because the pulse bias waveform is not significantly changed. Since the dc component of the bias signal is also blocked, larger pulse amplitude is required to produce zero-dc-biased operating margins. When the ac-coupled DCG inputs are used, there is insufficient pulse amplitude to achieve zero-crossing margins for the waveform with the large dc voltage, as shown in Fig. 5.

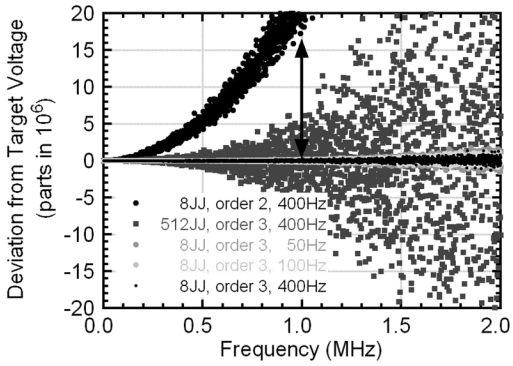

Fig. 6. Deviation from the "target" voltage of the magnitude of the synthesized tones for five delta–sigma modulated digital codes, including some that are shown in Fig. 5.

B. Optimized Waveforms

The QVNS circuit and waveform parameters can be optimized to ensure that the harmonic tone amplitudes of the digital codes match the target voltage to better than 1 $\mu\mathrm{V/V}$. The delta–sigma modulator algorithm generates digitization harmonics, as shown in Fig. 4. This same effect causes the tone amplitudes of the digitized waveform to deviate from the desired target amplitude. The magnitude of the deviations depends on the relative magnitude of the harmonic tones, the digitization harmonics, and the oversampling ratio. This effect became much more noticeable in 2005 when we increased our measurement bandwidth from 100 kHz to 650 kHz [10], [12].

The FFTs in Fig. 4 show that the digitization harmonics are 0.01 times as large at 1 MHz for the waveforms generated with the third-order modulator compared to those of the second-order modulator. Furthermore, the tone amplitudes for the 512 junction circuits are 1/64 large as those of the 8 junction circuit (both with $f_1 = 400\ \mathrm{Hz}$), as expected, which makes their tones much closer in magnitude to the digitization harmonics. The tone amplitudes also decrease as the square root of the pattern repetition frequency, as expected, for the three eight-junction patterns.

Fig. 6 shows the deviations of the harmonic amplitudes from their target voltages for five different digital codes. The deviations increase with frequency in a manner similar to that of the digitization harmonics. The smallest deviations occur for the smallest number of junctions (eight), the highest modulator order (three), and the largest tone spacing $(2f_1 = 800\ \mathrm{Hz})$. The codes reproduce the targeted voltage to within 1 part in 10^6 at frequencies below 1 MHz for the three third-order codes with $f_1 > 50\ \mathrm{Hz}$ that are designed for eight-junction circuits.

Fortunately, these deviations are calculable, and their values could be used to correct the measured frequency-dependent ratios of the resistor-to-QVNS spectral in the temperature measurements. However, it is much easier to reduce the number of junctions in the QVNS circuits and increase the modulator order to improve the amplitude targeting, so that our calculations don't require such corrections. The quadratic frequency response in the deviations for the second-order modulated waveform, as well as larger scatter for larger numbers of junctions (not shown), probably made it difficult to correctly match the transmission line frequency responses of the QVNS and the sense resistor for our measurements performed prior to 2005 [12]. In 2005, the optimum number of junctions was reduced from 512 to 20 or 8 in order to improve the voltage accuracy of the harmonics.

Unfortunately, the use of larger tone amplitudes to optimize voltage targeting conflicts with optimization of the waveforms for reducing the effects of distortion from nonlinearities in the measurement electronics. Previously [10], [12]–[14], it was shown that smaller tone amplitudes, which can be synthesized with larger tone densities and longer codes, produce considerably smaller distortion from the same nonlinearity. Early in the NIST JNT experiment, code generator memory size limited the code length and the pattern repetition frequency to 1589.5 Hz. Fortunately, newer code generators have larger memory and can now produce longer codes that can produce higher harmonic tone densities, so that the tones can have smaller amplitudes. The resulting smaller distortion improves overall JNT measurement performance, including reducing the measurement uncertainty. The typical waveform and circuit parameters described above are adequately optimized for both waveform accuracy and sufficiently small nonlinearities for our present 650 kHz measurement bandwidth.

V. Conclusion

Optimizing the codes and circuits for accurate amplitude targeting requires higher-order modulator algorithms (3rd), smaller numbers of junctions (eight), and larger-amplitude tones. Minimization of nonlinearities requires a high density of tones with correspondingly small amplitudes. Increasing the measurement bandwidth above 1 MHz, which is planned in the coming year, will further constrain the targeting accuracy. In order to maintain the low distortion and good voltage targeting, we will probably reduce the number of junctions to either four or only 2!

Acknowledgment

We thank all our JNT collaborators, including Sae Woo Nam, John Martinis, Wes Tew, Rod White, Jifeng Qu, Horst Rogalla, Alessio Polarollo, Chiharu Urano, and Norm Bergren, and Carl Williams for support of the NIST JNT/Boltzmann constant program.

REFERENCES

[1] S. P. Benz and C. A. Hamilton, "A pulse-driven programmable Josephson voltage standard," *Appl. Phys. Lett.*, vol. 68, pp. 3171–3173, May 1996.

[2] S. P. Benz and C. A. Hamilton, "Application of the Josephson effect to voltage metrology," *Proc. of the IEEE—Invited paper*, vol. 92, pp. 1617–1629, Oct. 2004.

[3] S. P. Benz, P. D. Dresselhaus, A. Rüfenacht, N. F. Bergren, J. R. Kinard, and R. P. Landim, "Progress toward a 1 V pulse-driven ac Josephson voltage standard," *IEEE Trans. Inst. Meas.*, vol. 58, pp. 838–843, Apr. 2009.

[4] S. P. Benz, J. M. Martinis, S. W. Nam, W. L. Tew, and D. R. White, "A new approach to Johnson noise thermometry using a Josephson quantized voltage source for calibration," in *Proceedings of TEMPMEKO 2001*, B. Fellmuth, J. Seidel, and G. Scholz, Eds., Berlin, Apr. 2002, pp. 37–44, VDE Verlag.

[5] S. Nam, S. Benz, P. D. Dresselhaus, W. L. Tew, D. R. White, and J. Martinis, "Johnson noise thermometry measurements using a quantized voltage noise source for calibration," *IEEE Trans. Inst. Meas.*, vol. 52, pp. 550–554, Apr. 2003.

[6] S. P. Benz, P. D. Dresselhaus, and J. Martinis, "An ac Josephson source for Johnson noise thermometry," *IEEE Trans. Inst. Meas.*, vol. 52, pp. 545–549, Apr. 2003.

[7] D. R. White, R. Galleano, A. Actis, H. Brixy, M. De Groot, J. Dubbeldam, A. L. Reesink, F. Edler, H. Sakurai, R. L. Shepard, and J. C. Gallop, "The status of Johnson noise thermometry," *Metrologia*, vol. 33, pp. 325–335, Aug. 1996.

[8] W. L. Tew, S. P. Benz, P. D. Dresselhaus, H. Rogalla, D. R. White, and J. R. Labenski, "Recent Progress in Noise Thermometry at 505 K and 693 K using Quantized Voltage Noise Ratio Spectra," in *Proceedings of TEMPMEKO & ISHM 2010*, Portoro, Slovenia, May 31–Jun. 4 2010, Joint International Symposium on Temperature, Humidity, Moistureand Thermal Measurements in Industry and Science.

[9] S. P. Benz, D. R. White, J. Qu, H. Rogalla, and W. L. Tew, "Electronic measurement of the Boltzmann constant with a quantum-voltage-calibrated Johnson-noise thermometer," *Experimental determination of the Boltzmann constant, Comptes rendus de l'Academie des Sciences*, vol. 10, pp. 849–858, Nov. 2009, 10.1016/j.physletb.2003.10.071, special issue on the .

[10] D. R. White and S. P. Benz, "Constraints on a synthetic-noise source for Johnson noise thermometry," *Metrologia*, vol. 45, pp. 93–101, Jan. 2008.

[11] D. R. White, S. P. Benz, J. R. Labenski, S. W. Nam, J. F. Qu, H. Rogalla, and W. L. Tew, "Measurement time and statistics for a noise thermometer with a synthetic-noise reference," *Metrologia*, vol. 45, pp. 395–405, Jul. 2008.

[12] S. P. Benz, J. Qu, H. Rogalla, D. R. White, P. D. Dresselhaus, W. L. Tew, and S. W. Nam, "Improvements in the NIST Johnson noise thermometry system," *IEEE Trans. Inst. Meas.*, vol. 58, pp. 884–890, Apr. 2009.

[13] R. C. Toonen and S. P. Benz, "Nonlinear behavior of electronic components characterized with precision multitones from a Josephson arbitrary waveform synthesizer," *IEEE Trans. Appl. Supercond.*, vol. 19, pp. 715–718, Jun. 2009.

[14] J. Qu, S. P. Benz, H. Rogalla, and D. R. White, "Reduced nonlinearities and improved temperature measurements for the NIST Johnson noise thermometer," *Metrologia*, vol. 46, pp. 512–524, 2009.

[15] A. Pollarolo, J. Qu, H. Rogalla, P. D. Dresselhaus, and S. P. Benz, "Development of a four-channel system for Johnson noise thermometry," *IEEE Trans. Instrum. Meas.*, to be published.

[16] J. Qu, S. P. Benz, A. Pollarolo, and H. Rogalla, "Reduced nonlinearities in the NIST Johnson noise thermometry system," *IEEE Trans. Instrum. Meas.*, to be published.

[17] H. Brixy *et al., Temperature, Its Measurement and Control in Science and Industry*, J. Schooley, Ed. *et al.* New York: American Institute of Physics, 1992, vol. 6, pp. 993–996.

[18] N. Hadacek, P. D. Dresselhaus, and S. P. Benz, "Lumped 50- Ω arrays of SNS Josephson junctions," *IEEE Trans. Appl. Supercond.*, vol. 16, pp. 2005–2010, Dec. 2006.

[19] M. Watanabe, P. D. Dresselhaus, and S. P. Benz, "Resonance-free low-pass filters for the ac Josephson voltage standard," *IEEE Trans. Appl. Supercond.*, vol. 16, pp. 49–53, Mar. 2006.

[20] C. J. Burroughs, S. P. Benz, P. D. Dresselhaus, Y. Chong, and H. Yamamori, "Flexible Cryo-packages for Josephson devices," *IEEE Trans. Appl. Supercond.*, vol. 15, no. 2, pp. 465–468, Jun. 2005.

[21] J. C. Candy, "An overview of basic concepts," in *Delta–Sigma Data Converters: Theory, Design, and Simulation*, S. R. Norsworthy, R. Schreier, and G. C. Temes, Eds. Piscataway, NJ: IEEE Press, 1997.